Front. Earth Sci. 2013, 7(4): 456–464
DOI 10.1007/s11707-013-0361-3

RESEARCH ARTICLE

# Global detection of large lunar craters based on the CE-1 digital elevation model

**Lei LUO[1,2], Lingli MU[3], Xinyuan WANG (✉)[1], Chao LI[1,2], Wei JI[1], Jinjin ZHAO[2,3], Heng CAI[1,2]**

1 Key Laboratory of Digital Earth Sciences, Institute of Remote Sensing and Digital Earth, Chinese Academy of Sciences, Beijing 100094, China
2 University of Chinese Academy of Sciences, Beijing 100049, China
3 National Astronomical Observatories, Chinese Academy of Sciences, Beijing 100012, China



**Abstract** Craters, one of the most significant features of the lunar surface, have been widely researched because they offer us the relative age of the surface unit as well as crucial geological information. Research on crater detection algorithms (CDAs) of the Moon and other planetary bodies has concentrated on detecting them from imagery data, but the computational cost of detecting large craters using images makes these CDAs impractical. This paper presents a new approach to crater detection that utilizes a digital elevation model instead of images; this enables fully automatic global detection of large craters. Craters were delineated by terrain attributes, and then thresholding maps of terrain attributes were used to transform topographic data into a binary image, finally craters were detected by using the Hough Transform from the binary image. By using the proposed algorithm, we produced a catalog of all craters $\geqslant$10 km in diameter on the lunar surface and analyzed their distribution and population characteristics.

**Keywords** digital elevation model, crater detection algorithm (CDA), curvature, Hough Transform, CE-1

## 1 Introduction

A central characteristic of the lunar surface, craters are concave terrain features generated by meteorite impacts or volcanic activity. The moon has no atmosphere, so craters play an important role in studies of the morphology of the lunar surface, the structure of lunar rock, and the origin of the moon (Neukum et al., 1975; Ivanov et al., 2002; Ouyang, 2005; Ouyang et al., 2010). In most recent studies, target craters have had to be manually extracted from images, though there have been some automatic or semiautomatic crater detection algorithms proposed (Di et al., 2002; Honda et al., 2002; Alves, 2003; Earl et al., 2005; Sawabe et al., 2006; Yue et al., 2008; Bandeira et al., 2010). This is a difficult task because of the inherent limitations of imagery data and the variety of crater structures (Bue and Stepinski, 2007). Some craters are degraded by erosion and are barely distinguishable from the background data.

Image-based crater detection approaches involve complicated, multi-step algorithms to combat the inherent limitations of imagery data. For example, Sawabe et al. (2006) used multiple boundary-based approaches and merged the results obtained. In Kim et al. (2005), detected craters were verified by template matching and neural networks were employed to remove false detections. In Magee et al. (2003), different algorithms were combined to improve the detection rate. In spite of these sophistications, image-based crater detection algorithms had only limited success. In summary, it is not easy for those algorithms to detect craters when the terrain becomes complex.

Presently, several digital elevation model (DEM)-based detection algorithms, a supplement to imagery data in detecting large craters, were used for Mars and other planetary bodies (Kim et al., 2005; Bue and Stepinski, 2007; Salamuniccar and Loncaric, 2010). In this study, an improved DEM-based detection algorithm was used to detect global large lunar craters from Chang'E-1(CE-1) DEM. First, we establish that topographic slope and profile curvature are the preferred terrain parameters to extract topographic rims. Second, we devise a method of detecting the craters rims with an advanced Hough Transform. Third, we give a confirmation function to remove the false detection that supplements the Hough Transform in identifying circular features in a noisy binary image. By using this proposed algorithm, we produced a catalog of all craters $\geqslant$10 km in diameter on the lunar surface.

Received December 12, 2012; accepted January 1, 2013

E-mail: xywang@ceode.ac.cn

## 2 Data

The Laser Altimeter (LAM), an instrument on board the CE-1 satellite, has acquired globally distributed, high-precision measurements of the topography of the Moon from November 28, 2007 to December 4, 2008, which enable the creation of a 64-pixels-per-degree DEM (see Fig. 1) and a shaded relief model of the surface. The LAM obtained more than nine million range measurements in total during one year of observation. Li et al. (2010) used those data, covering the entire lunar surface, to make a complete lunar DEM. The plane positioning accuracy of the lunar DEM is 445 m and height determination accuracy is 60 m. The DEM data was constructed by using Kriging interpolation (Li et al., 2010) and a 500 m resolution coordinate grid.

These data provide a view of the global distribution of craters without the observational uncertainties that arise from detection of craters on images of heterogeneous illumination conditions and uneven coverage and quality. We used our proposed crater detection algorithm to produce a global catalog of the craters $\geqslant$10 km in diameter based on this data set.

Based on the requirement of the data resolution and detecting computation, in this study, the DEM of the Moon is divided into 188 subdivisions according to longitude and latitude (Li et al., 2013). The polar regions of 84°–90° are assigned as two whole DEMs, respectively (see Fig. 2). The areas of 84°N –84°S, along with the latitude direction, in accordance with every 14° interval, are divided into 12 projected sub-zones. In each sub-zone, from the high latitude to the equator, the longitudes of 45°, 30°, 24°, 20°, and 18° are chosen as each longitudinal extent of each separated subdivision DEM, separating the area between 84°N and 84°S into 186 subdivisions. Thus, in all, the Moon surface is divided into 188 subdivisions.

## 3 Method

### 3.1 Slope and profile curvature

The lunar surface, represented by the DEM, has varying curvatures in different directions. Bue and Stepinski (2007) used the values of $k(x, y)$ to delineate craters from the Martian DEM. In our application, the slope, $s(x, y)$, is a useful feature for delineating crater walls and rims and profile curvature (Michael et al., 2003; Kim et al., 2005). The value of $k(x, y)$ is of interest because it measures the change of slope angle. Profile curvature is used to distinguish between convex and concave crater walls and ridges; $k > 0$ corresponds to convex topography, whereas $k < 0$ corresponds to concave topography.

However, slope, $s(x, y)$, is an inferior rim indicator, especially for smaller or more degraded craters. In addition to slope, we have investigated profile curvature, $k(x, y)$, as a rim indicator, which was used by Bue and Stepinski (2007). Indeed, we have found that $k$ is not the best terrain attribute to outline a broad range of lunar crater types, and we have selected a new indicator, a combination of slope and curvature $sk(x, y)$, to define the rims of lunar craters in our algorithm. The $sk(x, y)$ is defined as follows:

$$sk(x,y) = s(x,y) \times k(x,y). \quad (1)$$

In this study, we used the Hough Transform to identify craters in a terrain attributes map. However, the Hough Transform by itself is not effective because of the large number of false detections. We used the Hough Transform

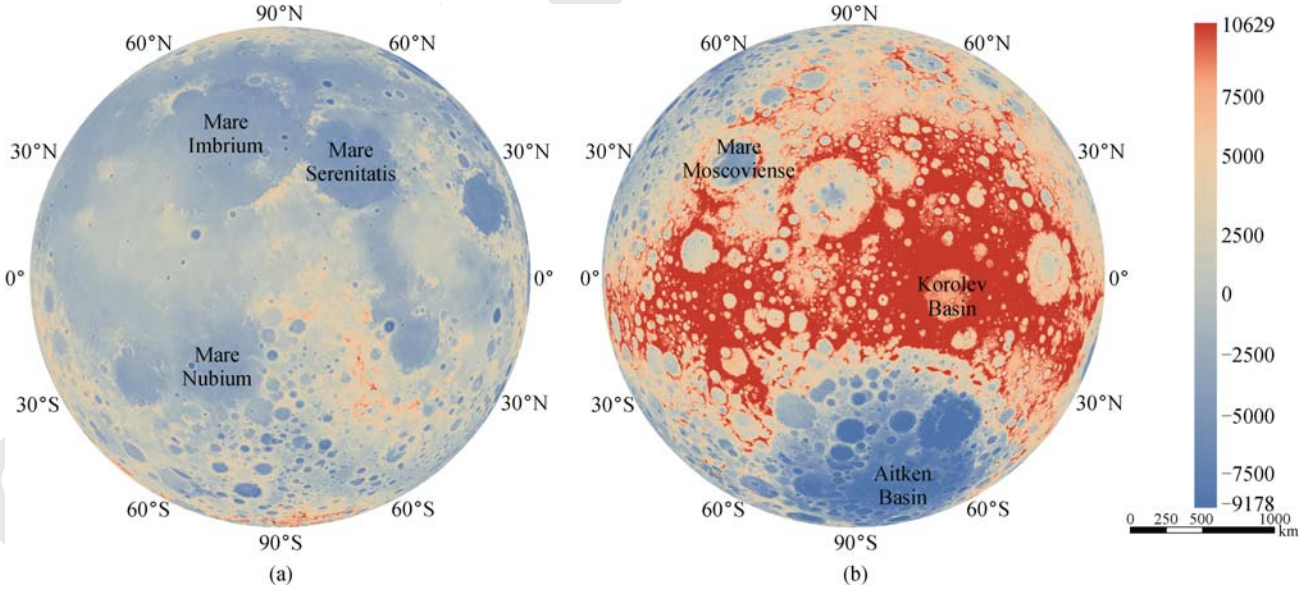


**Fig. 1** Global lunar DEM model mapped with CE-1 LAM data. (a) is the DEM model of the near side, and (b) is the far side.

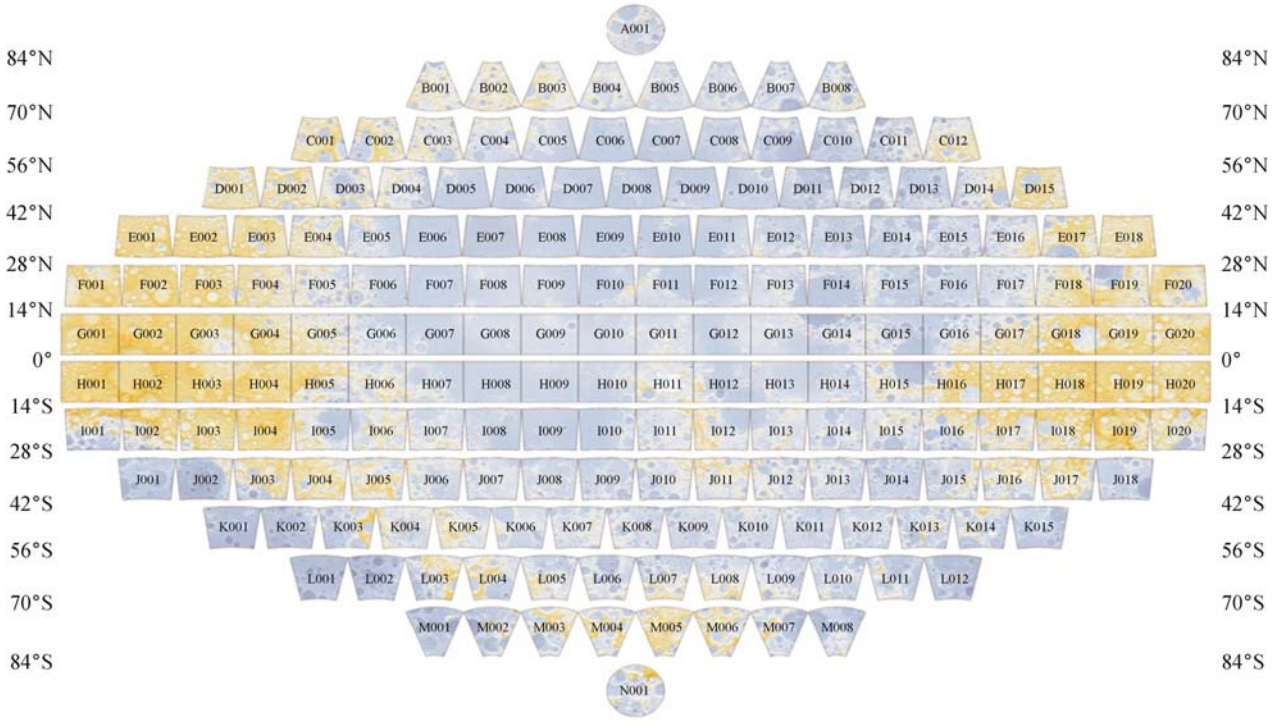


**Fig. 2** Code of the subdivision topographic maps of the Moon.

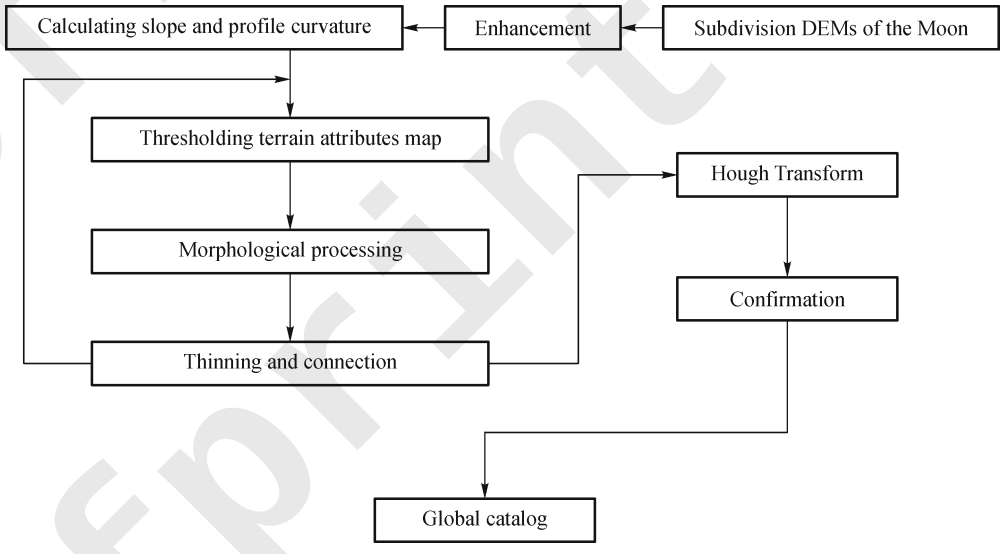


**Fig. 3** Flowchart of the crater detection algorithm.

to produce a list of crater candidates. Moreover, a confirmation algorithm was designed to remove false detections (Luo et al., 2011). Figure 3 shows the overall structure of the DEM-based lunar crater detection algorithm.

### 3.2 Identifying crater rims

The DEM representation of the lunar surface lacks smoothness because of accuracy, resolution, interpolation, and the true roughness of the lunar landscape. Calculating terrain attributes directly from the DEM would produce results too noisy for reliable delineation of craters. For this reason, we smooth the lunar subdivision DEMs using the median filter. The results of calculating $s$ for the G016 are shown in Fig. 4(b). The values of $s$ between the minimum values (0), which correspond to the crater rims, are depicted in black, and values to the maximum positive

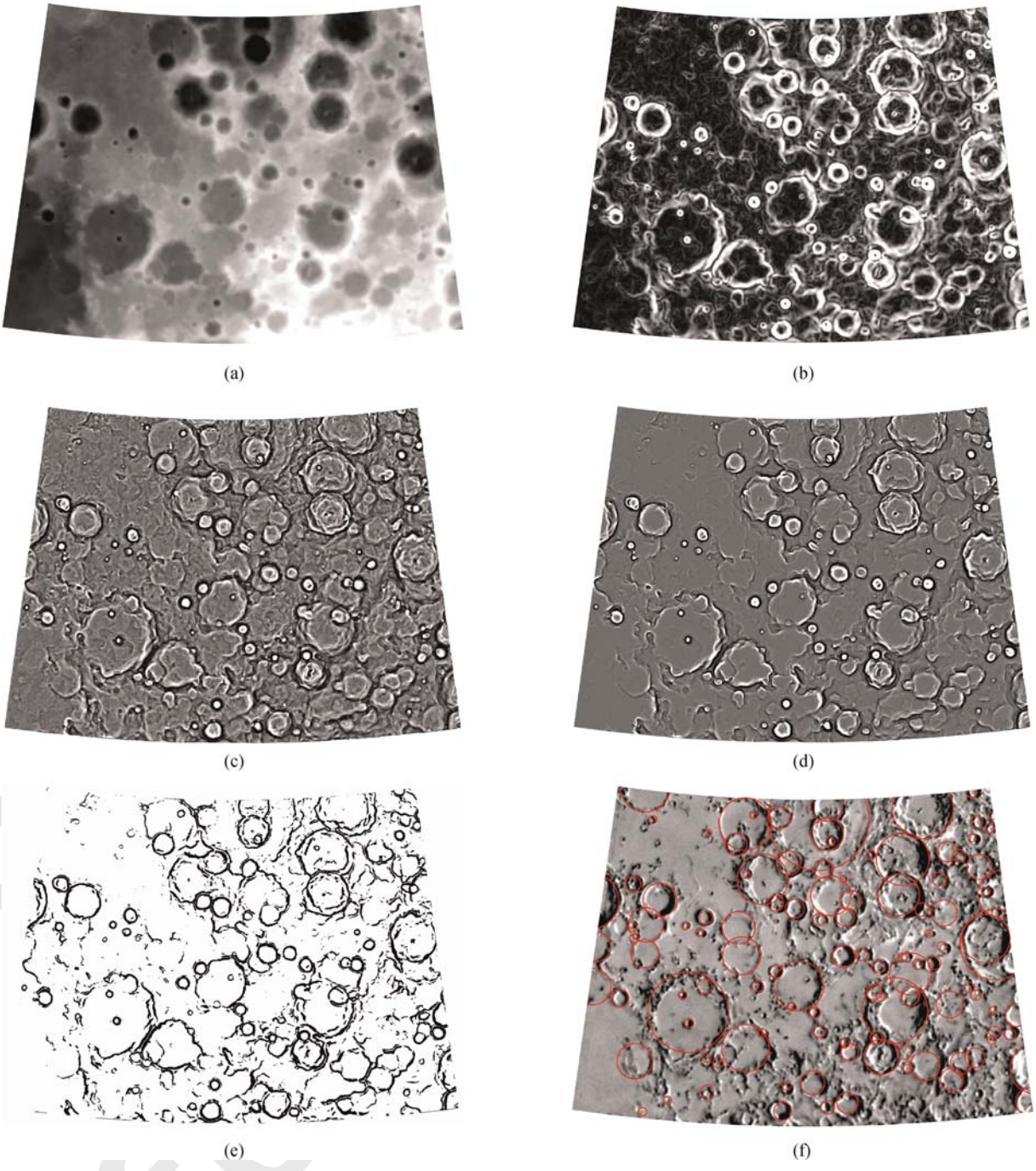


**Fig. 4** (a) Subdivision DEM with code of G016. (b) The values of slope in the test site from 0 (rims), shown in black, to 40.53 (walls), shown in white. (c) The grayscale gradient depicts values of profile curvature in the test site from –0.138 (concave areas), shown in black, to +0.152 (convex areas), shown in white. (d) The values of $sk$ ($x$, $y$) in the test site from large negative (concave areas), shown in black, to large positive (convex areas), shown in white. (e) The binary image of the test site showing the areas with $sk \leqslant -0.02$). (f) The detection results were shown on top of a shade relief of the DEM with red circles.

( +40.53), which correspond to crater walls, are depicted in white. The results of calculating $k$ for the test site are shown in Fig. 4(c). The grayscale gradient indicates values of $k$ between the maximum negative (−0.138), corresponding to the most concave areas, and are depicted in black, and values to the maximum positive (+ 0.152), corresponding to most convex areas, are depicted in white.

The results of calculating $sk$ for the test site are shown in Fig. 4(d). The values of $sk$ between the maximum negative (− 1.433) correspond to the most concave areas and are depicted in black, and values to the maximum positive (+ 1.485) correspond to the most convex areas and are depicted in white. Comparing Fig. 4(d) to Fig. 4(c) indicates that the $sk(x,y)$ map, with some noise, is better

than $k(x,y)$, but does not present a major obstacle to crater detection since its spatial distribution does not display circular features.We use the values of $sk(x,y)$ to produce a binary image, $I_{sk}(x,y)$, of the site according to the following transformation:

$$I_{sk(x,y)} = \begin{cases} 1(\text{black}), & sk(x,y) \leqslant sk_{th}, \\ 0(\text{white}), & sk(x,y) > sk_{th}. \end{cases} \quad (2)$$

Here, $sk_{th}$ is a threshold value for concave areas. The chosen value of $sk_{th}$ represents a tradeoff between selectivity and the presence of noise. We have chosen to use a relatively large value of $sk_{th} = -0.02$ in order to increase detection chances for small or degraded craters. Figure 4(e) shows the final binary image of the threshold profile curvature constructed for our test site. Comparing Figs. 4(a)–4(e) indicates that a combination of slope and profile curvature has delineated most craters in the DEM.

### 3.3 Hough Transform and confirmation

During the work on the new catalog, we used a crater detection algorithm (CDA) in order to propose crater candidates. The new DEM-based CDA is based on previous work (Luo et al., 2011; Li et al., 2012), and relies on a specially developed interpolation method which is suitable for detection of large craters. We extract the craters from the binary image by using the Hough Transform and confirmation. The Hough Transform from the previous work (Luo et al., 2011) utilizes improved canny edge detection, followed by morphological processing. The results of the crater detection are shown in Fig. 4(f).

## 4 Results

### 4.1 Global detection results

Two Lunar catalogs developed by previous researchers are: (i) The McDowell (2007) catalog, which contains 8639 (named) craters; and (ii) The Rodionova et al. (1987) catalog, which is one of the most complete catalogs of Lunar large craters, containing14923 craters (1394 identified by name). An additional Lunar catalog (Head et al., 2010; Kadish et al., 2011), which contains 5185 craters $\geqslant$20 km in diameter was developed by manual extraction.

Figure 5 (a) shows the results of DEM-based automatic crater detection. The color rendering of the CE-1 DEM shows detected craters as circles of black. The projection adopts the Mollweide homalographic pseudo cylindrical mode, and the central meridian adopts 0° with the central as the front of the Moon. The previous studies have a manual count of 14923 craters $\geqslant$10 km in diameter on the surface of the Moon (Rodionova et al., 1987). Our DEM-based crater detection algorithm has identified 15821craters, and 14394 craters are true. There were 14 craters identified by manual extraction but are absent from our algorithm (see Table 1). The majority of these missed craters are large impact basins and mares, especially Orientale and Imbrium, showing no sharp rims.

**Table 1** Comparison of Rodionova et al. (1987) to our CAD

| Diameter | Our CAD | LU14923 | LU5185 |
|---|---|---|---|
| 10–20 | 10524(9518) | 8901 | 0 |
| 20–40 | 3077(2656) | 3920 | 2951 |
| 40–80 | 1634 | 1608 | 1634 |
| 80–160 | 498 | 419 | 498 |
| >160 | 88 | 75 | 102 |

### 4.2 Crater densities on the Moon

By using the detection results, we determined the areal density of craters on the Moon by calculating the number of craters in a moving neighborhood of 500 km in radius (Fig. 5 (b)).The resulting crater densities reflect first-order variations in the crater retention age (for 10 km craters and larger) across the surface. We report densities here as $N(10)$ values, which represent the number of craters per unit area with diameter $\geqslant$10 km, normalized to $10^6$ km$^2$.

The spatial distributions (see Fig. 5 (a)) for global large lunar craters are used to reveal potential spatial heterogeneity based on our CAD. The spatial heterogeneity is mainly embodied in the following aspects: (i) the craters with larger diameters, especially the multi-ring impact basin, dominantly distributed in the highland and show obvious concentration tendency. However, (ii) the mare regions have fewer larger craters, accompanied by numerous smaller craters, and (iii) larger craters have the characteristics of randomness and the smaller crater are concentrated in local areas. The most prominent features in Fig. 5 (b) are (iv) the densely cratered highlands, particularly on the southern near side and north-central far side of the Moon, (v) the interior and surroundings of stratigraphically young impact basins, especially Orientale, and (vi) mare regions, which have the lowest crater densities on the Moon.

### 4.3 Crater SFD analysis

There have been many studies of the cumulative size-frequency distribution (SFD) of lunar craters. In this study, the cumulative frequency method can also be used to study size distributions of the craters. The cumulative crater distributions measured on geological units of various age could be aligned along a contiguous complex curve with vertical shifts (Neukum et al., 1975; Neukum and Ivanov, 1994). Approximation of the normalized logarithmic cumulative frequencies with an 11$^{th}$ degree polynomial in log$D$ fits the complex structure of the distribution with sufficient accuracy (Neukum et al., 2001; Ivanov et al., 2002). The polynomial has the form:

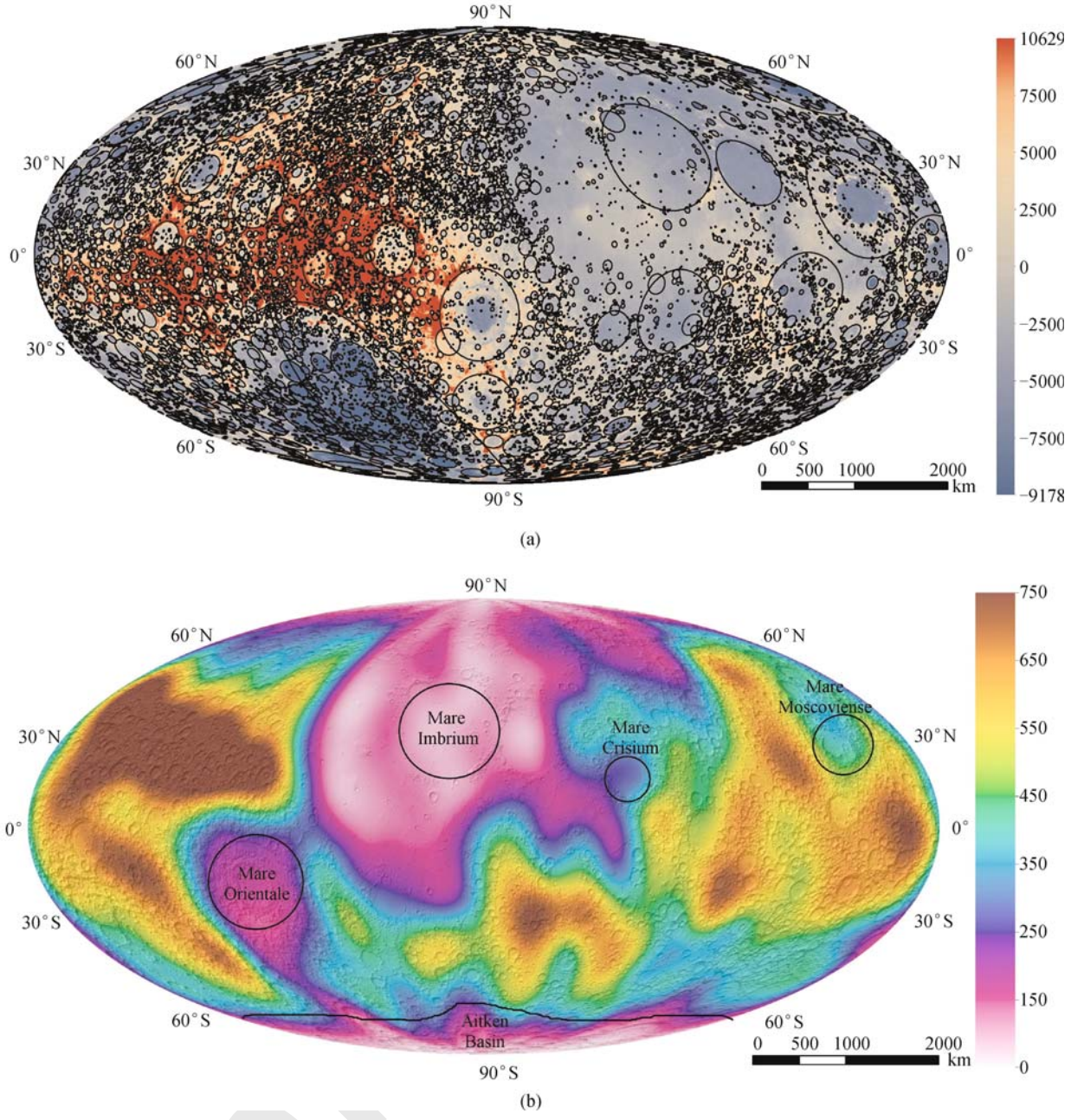


**Fig. 5** (a) Global detected lunar large craters ($\geqslant 10$ km in diameter) shown on top of a color rendering of CE-1 DEM. (b) Crater densities on the Moon for craters $\geqslant 10$ km in diameter, calculated in neighborhoods of radius 500 km.

$$\log N = a_0 + \sum_{n=1}^{11} a_n (\log D)^n, \quad (3)$$

where $D$ is a diameter of the crater in km and $N$ is the number of craters per km$^2$. Here $a_0$ represents the intercept at 1 km in diameter. Eq. (3) coefficients are as follows:

$a_1 = -3.557528,\ a_2 = 0.781027,\ a_3 = 1.021521,$
$a_4 = -0.156012,\ a_5 = -0.444058,\ a_6 = 0.019977,$
$a_7 = 0.086850,\ a_8 = 0.005874,\ a_9 = 0.006809,$
$a_{10} = 0.000825,\ a_{11} = 0.0000554.$

The empirically derived chronology by Neukum and Ivanov (1994) is given by:

$$N_{\mathrm{cum}}(D \geqslant 1\mathrm{km}) = 5.44 \times 10^{-14}\{\exp(6.93t) - 1\} + 8.38 \times 10^{-4} t, \quad (4)$$

where $t$ is time in billions of years.

In this study, Eqs. (3) and (4) were used to fit the crater detections by the least-square method and calculate surface absolute ages.

The cumulative frequency curve of these 14394 craters, $\geqslant 10$ km in diameter, is shown in Fig. 6(a). Figure 6(b)

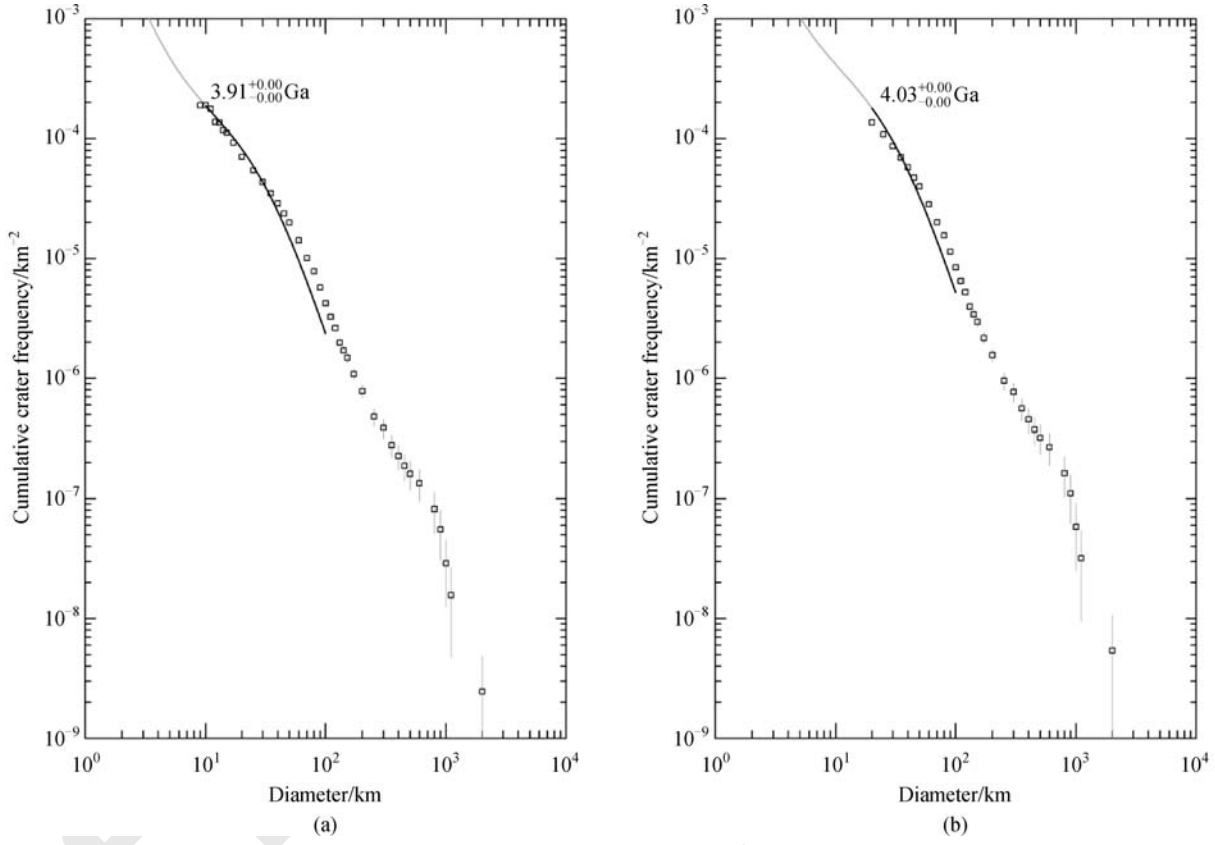


**Fig. 6** Cumulative size–frequency distribution of global detection results of CE-1 DEM. (a) SFD for craters ⩾10 km in diameter, (b) SFD for craters ⩾20 km in diameter.

shows the craters ⩾20 km in diameter. The cumulative frequency curve for each set is simulated to identify the relationship between crater numbers on the lunar surface and the diameter size distribution. The measured cumulative crater frequencies are used to obtain a general calibration size distribution curve by a normalization procedure. It is found that the lunar crater size distribution is largely constant in the size range 10 km⩽$D$⩽ INF for global surface with formation ages is ~3.9 Ga.

The formation ages in this study are between ~3.9 Ga and more than 4.0 Ga from extracted craters, whereas the ages from the Neukum et al. (1975) data are between ~3.0 Ga and more than 4.0 Ga. Tremendous similarities are found between these two studies. The difference in the studies shows that craters with small diameters are absent. These small impact craters are mainly secondary craters (McEwen and Bierhaus, 2006; Wan et al., 2012). It also can be seen from the scatter diagram that craters with diameters smaller than 10 km cannot be extracted reproducibly, probably due to the resolution of the data.

## 5 Discussion and conclusions

In this study, we have presented a comprehensive method for detecting global large lunar craters from topographic data. Although our input is DEM data, the actual crater detection is performed from binary images resulting from thresholding image maps of a combination of slope and profile curvature. Thus, the relative simplicity of our algorithm in comparison with image-based algorithms can be attributed to working with binary instead of grayscale images because detecting craters from DEMs is more efficient than detecting them from images. In comparison with the study of predecessors, the novel extraction method presented in this study can also obtain a certain number of craters accurately, which proves the viability of the CE-1 DEM data. In addition, some ancient impact basins from the early Imbriam could have been destroyed and hence cannot be extracted. This paper focuses only on the detection of large lunar craters; future research will address sub-kilometer craters.

Drawing a comparison between our detections and Neukum et al. (1975) crater counts via the crater chronology, the accuracy of the novel detected method was demonstrated. By analyzing the distribution and population characteristics of the craters, it is shown that the lunar surface has large numbers of large craters, but the spatial pattern of these craters shows marked regional differentiation characteristics, and the relationship between

the pattern and the crater forming theory requires further study before the ultimate goal can be reached.

The deviation of size and location of detection craters will be improved in the future, and adding the properties to craters by using the information in CE-1 and CE-2. An extraction and analysis system will be built which base on the information of craters. Craters detected by DEM-based CAD also can be used in further research on Mars, for instance, estimating Martian surface geology and relative age.

**Acknowledgements** We express our gratitude to the National Astronomical Observatories, Chinese Academy of Sciences, which offered the data for this study. This work was supported by the National Hi-Tech Research and Development Program of China (Grant No. 2010AA122202 – 02) and the National Natural Science Foundation of China (Grant No. 60972141)

## References

Alves E I (2003). A New Crater Recognition Method and Its Application to Images of Mars. In: Geophysical Research Abstracts. Nice: Copernicus Publications

Bandeira L, Ding W, Stepinski T F (2010). Automatic detection of sub-km craters using shape and texture in formation. In: Proceedings of the 41st Lunar and Planetary Science Conference, Abs. 1144, March 1–5, 2010, Houston, US

Bue B D, Stepinski T F (2007). Machine detection of Martian impact craters from digital topography data. IEEE Trans Geosci Rem Sens, 45(1): 265–274

Di S F, Costantini M, DiMartino M (2002). Craters — Executive summary: survey of algorithms for automatic recognition of impact craters. ESA Contract Report, Paris, France

Earl J, Chicarro A, Koeberl C, Marchetti P G, Milnes M (2005). Automatic recognition of crater-like structures in terrestrial and planetary images. In: Proceedings of the 36th Lunar and Planetary Science Conference, Abs.1319, March 14–18, 2005, Houston, US

Head J W Ⅲ, Fassett C I, Kadish S J, Smith D E, Zuber M T, Neumann G A, Mazarico E (2010). Global distribution of large lunar craters: implications for resurfacing and impactor populations. Science, 329 (5998): 1504–1507

Honda R, Iijima Y, Konishi O (2002). Mining of topographic feature from heterogeneous imagery and its application to lunar craters. Lecture Notes in Computer Science, 2281: 395–407

Ivanov B A, Neukum G, Bottke W F, Hartmann W K (2002). The Comparison of Size-Distributions of Impact Craters and Asteroids and the Planetary Cratering Rate, Asteroids III. Tucson: University of Arizona Press

Kadish S J, Fassett C I, Head J W, Smith D E, Zuber M T, Neumann G A, Mazarico E (2011). A global catalog of large Lunar craters (⩾ 20 km) from the Lunar Orbiter Laser Altimeter. In: Proceedings of the 42nd Lunar and Planetary Science Conference, Abs. 1006, March 7–11, 2011, Houston, US

Kim J R, Muller J P, Stephan S V, Morley J G, Neukum G (2005). Automated crater detection, a new tool for Mars cartography and chronology. Photogrammetric Engineering & Remote Sensing, 71: 1205–1217

Li C L, Liu J J, Mu L L, Ren X (2013). The Chang'E-1 Topographic Atlas of the Moon. Beijing: SinoMaps Press (in Chinese)

Li C L, Ren X, Liu J J, Zou X D, Mu L L, Wang J Y, Shu R, Zou Y L, Zhang H B, Lü C, Liu J Z, Zuo W, Su Y, Wen W B, Bian W, Wang M, Xu C, Kong D Q, Wang X Q, Wang F, Geng L, Zhang Z B, Zheng L, Zhu X Y, Li J D, Ouyang Z Y (2010). Laser altimetry data of Chang'E-1 and the global lunar DEM model. Science China–Earth Sciences, 53(11): 1582–1593

Li C, Wang X Y, Luo L, Ji W (2012). Automatic detection of lunar elliptical craters from Apollo Image. Remote Sensing for Land & Resources, 95: 71–75 (in Chinese)

Luo L, Wang X Y, Ji W, Li C (2011). Automated detection of lunar craters based on Chang'E-1 CCD data. In: Qiu P H, Xiang Y, Ding Y S, Li D M, Wang L P, eds. Proceedings of the 4th International Congress on Image and Signal Processing. Shanghai: Donghua University

Magee M, Chapman C R, Dellenback S W, Enke B, Merline W J, Rigney M P (2003). Automated identification of Martian craters using image processing. In: Proceedings of the 34th Lunar and Planetary Science Conference, Abs. 1756, March 17–21, 2003, Houston, US

McDowell J (2007). Lunar Nomenclature. Jonathan's Space Report

McEwen A S, Bierhaus E B (2006). The importance of secondary cratering to age constraints on planetary surfaces. Annual Review of Earth and Planetary Sciences, 34(1): 535–567

Michael G G (2003). Coordinate registration by automated crater recognition. Planetary and Space Science, 51(9–10): 563–568

Neukum G, Ivanov B A (1994). Crater size distributions and impact probabilities on earth from lunar terrestrial-planet, and asteroid cratering data, Hazards Due to Comets and Asteroids. Arizona: University of Arizona

Neukum G, Ivanov B, Hartmann W K (2001). Cratering records in the inner solar system in relation to the lunar reference system. Space Science Reviews, 96: 55–86

Neukum G, Konig B, Arkani J H (1975). A study of lunar impact crater size-distributions. Moon, 12: 201–229

Ouyang Z Y (2005). Introduction to Lunar Science. Beijing: China Aerospace Press (in Chinese)

Ouyang Z Y, Li C L, Zou Y L, Zhang H B, Lü C, Liu J Z, Liu J J, Zuo W, Su Y, Wen W B, Bian W, Zhao B C, Wang J Y, Yang J F, Chang J, Wang H Y, Zhang X H, Wang S J, Wang M, Ren X, Mu L L, Kong D Q, Wang X Q, Wang F, Geng L, Zhang Z B, Zheng L, Zhu X Y, Zheng Y C, Li J D, Zou X D, Xu C, Shi S B, Gao Y F, Gao G N (2010). Primary scientific results of Chang'E-1 Lunar mission. Science China-Earth Sciences, 53(11): 1565–1581

Rodionova J F, Karlov A A, Skobeleva T P, Konotopskaya E V, Shevchenko V V, Kozubskiy K E, Dekhtyareva K I, Smolyakova T F, Tishik L I, Fedorova E A (1987). Morphological Catalogue of the Craters of the Moon. Moscow: Mosk Gos Univ Press

Salamuniccar G, Loncaric S (2010). Method for crater detection fron Martian digital topography data using gradient value/orientation, morphometry, votes-analysis, slip-tuning and calibration. IEEE Trans Geosci Rem Sens, 48(5): 2317–2329

Sawabe Y, Matsunaga T, Rokugawa S (2006). Automated detection and classification of lunar craters using multiple approaches. Advances in Space Research, 37(1): 21–27

Wan C, Cheng W M, Zhou Z P, Zhao S M, Xia Y (2012). Automatic extraction of lunar impact craters from Chang'E-1 satellite photo-

graphs. Sci China Phys Mech Astron, 55(1): 162–169

Yue Z Y, Liu J Z, Wu G G (2008). Automated detection of lunar craters based on object-oriented approach. Chinese Science Bulletin, 53(23): 3699–3704

## AUTHOR BIOGRAPHIES

**Lei Luo** received his Bachelor degree in geography from Anhui Normal University, Wuhu, China in 2010. He currently is a Master Candidate of Institute of Remote Sensing and Digital Earth (RADI), Chinese Academy of Sciences, Beijing, China. His research interests involve Lunar and Planetary morphology, processing and analysis of remote sensing image and remote sensing in archaeology. He uses remote sensing and modeling to study Lunar and Earth cratering and impact on environments in the present. E-mail: lluo@ceode.ac.cn

**Xinyuan Wang** graduated from Beijing Normal University, Beijing, China in 1986 and received his Ph.D. degree at Nanjing University, Nanjing, China in 2000. Now, he is a Research Fellow of Institute of Remote Sensing and Digital Earth (RADI), Chinese Academy of Sciences, Deputy Director of the Key Laboratory of Digital Earth Sciences, Chinese Academy of Sciences, Beijing, China. His current research is on digital environmental archaeology, morphological analysis of Lunar and Planetary surface, Quaternary environmental change and space technologies for natural and cultural heritage, and their associated information technology and decision support systems. Professor Wang is a member of Chinese National Committee of the International Society for Digital Earth (CNISDE) and is responsible for the Digital Heritage. He is Deputy Director of the International Centre on Space and Technologies for Natural and Cultural Heritage (HIST), under the Auspices of UNESCO, and a member of the Committee for Digital Great Wall Program. E-mail: xywang@ceode.ac.cn